Integrating field observations and fracture mechanics models to constrain seismic source parameters for ancient earthquakes

W. Ashley Griffith[1] and Vikas Prakash[2]
[1]Department of Earth and Environmental Sciences, University of Texas at Arlington, Arlington, Texas 76019, USA
[2]Department of Mechanical and Aerospace Engineering, Case Western Reserve University, Cleveland, Ohio 44106, USA

ABSTRACT

Most of our understanding of earthquake rupture comes from interpretation of strong-ground-motion seismograms; however, near-rupture-tip fields of stress and particle motions are difficult to resolve. In particular, the decay of frictional resistance from a peak value at the leading tip of the rupture to a residual kinetic value and subsequent healing characterizes the earthquake process, yet the nature of this evolution in situ is still unclear. Knowledge of this coseismic frictional constitutive behavior has been supplemented by laboratory experiments, yet scaling laboratory experiments to natural faults is non-trivial because these experiments do not exactly reproduce the boundary conditions governing natural earthquakes. Field investigations of exhumed faults provide the spatial resolution needed to integrate remote seismological observations, laboratory experiments, and numerical models of the rupture process for natural ruptures. Here we build on previous work that showed that the orientation of pseudotachylyte injection veins found along the Gole Larghe fault zone in granitoid rocks of the Italian Alps can be used to infer rupture directivity and velocity. We demonstrate that the length of these veins can be used to further constrain the rupture size, slip weakening distance, stress drop, and fracture energy. The results are consistent with seismological observations and recent friction experiments incorporating rapid accelerations, placing constraints on coseismic frictional evolution in granitoid rocks.

INTRODUCTION

Most seismic source parameters, including stress and strength drop, fracture energy G, slip distance S, and rupture velocity v_{II}, are routinely estimated using seismology. Earthquake rupture requires frictional resistance on a fault to drop from a peak value equal to the static fault strength to a smaller residual value (i.e., strength drop) with slip, a process described as "slip weakening". The fracture energy $G(S)$, defined as the area under the shear stress–versus–slip curve between the peak and residual stresses, is a robust seismological measure; however, absolute stress values before and after slip, and the slip weakening distance D_c, are difficult to resolve (Abercrombie and Rice, 2005). During the past two decades, laboratory friction experiments conducted in different configurations have been employed to investigate coseismic frictional constitutive behavior of rocks and analog materials at or near seismic slip speeds (e.g., Yuan and Prakash, 2008a, 2008b; Di Toro et al., 2011). These studies provide valuable insight into the evolution of friction stress during slip, yet the broad validity of laboratory-derived frictional constitutive laws, particularly at fast slip rates, remains unclear. An obvious source of discrepancy comes from the fact that many of these experiments are conducted at normal stress and slip velocity that may not reflect conditions during natural seismic fault ruptures (Niemeijer et al., 2012; Rowe and Griffith, 2015).

Given the difficulty of resolving near-tip stress and velocity fields of earthquake ruptures and replicating natural seismic slip conditions in the laboratory, in the present study we use coseismically formed fault structures exposed along exhumed faults to characterize transient near-tip stress fields associated with ancient earthquakes. This approach builds off the work of Di Toro et al. (2005a) in which orientation and spatial distribution of pseudotachylyte injection veins along the Gole Larghe fault zone cutting tonalite in the southern Italian Alps were used to infer earthquake rupture velocity and directivity. We extend this approach by using the measured injection vein lengths to further constrain earthquake source parameters, including dynamic stress and strength drops, rupture pulse length, G, and D_c, using the pulse-like rupture model of Rice et al. (2005), an analytical model for the two-dimensional (2-D) stress field around a moving slip pulse of length L with a slip-weakening zone of length R behind the rupture tip. Figure 1 shows a schematic of the slip pulse propagating along a pre-cut interface in a laboratory specimen (Xia et al., 2004; Griffith et al., 2009). The model uses a moving coordinate system with the origin at the rupture tip and the positive x-axis in the direction of rupture (Fig. 1). Within the slip-weakening zone, shear stress experiences a spatially linear decay from peak τ_p to a residual value τ_r at the trailing edge of the slip weakening zone ($x = -R$). Slip occurs along the entire slip patch of length L, and the strength is assumed to recover at the trailing edge ($x = -L$). This decay has an exponential relationship with slip, i.e., $\tau(S) = (\tau_p - \tau_r)e^{(-S/D_c)} + \tau_r$, where D_c is a characteristic slip distance (Rice et al., 2005). Using this form, fracture energy G can be estimated by integrating over the first term on the right-hand side of this equation, yielding $G = (\tau_p - \tau_r) D_c$ for $D_c < S$. Note that this definition relationship differs from the commonly applied relationship $G = \frac{(\tau_p - \tau_r)}{2} D_c$ in which the relationship between stress and slip is assumed to be linear and no weakening occurs beyond the slip D_c (e.g., Abercrombie and Rice, 2005). It is assumed that the fault strength heals to its original value such that final fault strength $\sigma^f_{yx} = \sigma^0_{yx}$ for $x < -L$. The pulse model for earthquake rupture is convenient for the present application because the ratio of the dynamic stress drop ($\sigma^0_{yx} - \tau_r$) to the strength drop ($\tau_p - \tau_r$) is constrained by L/R, reducing the number of free variables (Rice et al., 2005, their equation 8). The model does not require knowledge of the frictional constitutive behavior *a priori*, and due of the relationship between L, R, and $\sigma^0_{yx} - \tau_r$, only a few combinations of these parameters can match the total slip magnitude constrained in the lab or field.

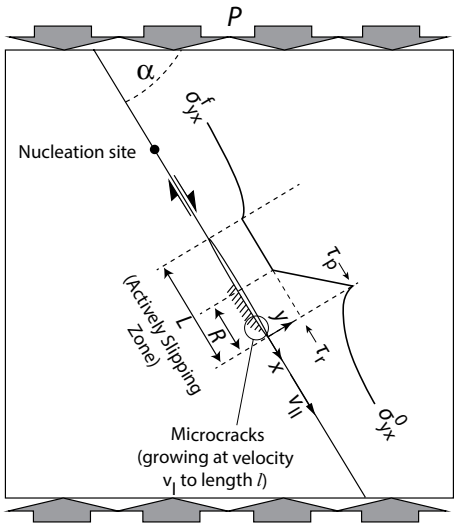

Figure 1. Parameters describing the Rice et al. (2005) slip pulse mode superimposed on experimental set-up of Griffith et al. (2009), with initial shear traction (σ^0_{yx}), peak strength (τ_p), residual sliding friction (τ_r), recovered frictional strength ($\sigma^f_{yx} = \sigma^0_{yx}$), fault orientation ($\alpha$), remote load ($P$), pulse length ($L$), and slip weakening zone length (R) defined schematically. Mode I and II rupture velocities are v_I and v_{II}, respectively. See text for discussion.

Di Toro et al. (2005a) used this model to study the orientation of pseudotachylyte injection veins along faults of the Gole Larghe fault zone. These veins grew in arrays preferentially along one side and at high angles to individual faults. Di Toro et al. (2005a) designed rupture scenarios producing coseismic slips of ~1.5 m with 5.6 MPa ≤ $(\sigma^0_{yx} - \tau_r) \leq 42$ MPa, constrained independently by considering the amount of work necessary to produce the volume of melt present along these faults (Di Toro et al., 2005b). The resulting ruptures were characterized by slip pulses of lengths 200 m ≤ L ≤ 1000 m, resulting in tensile regions with lengths 40–200 m along the moving rupture (Di Toro et al., 2005a). They concluded that a range of scenarios in which the rupture velocity v_{II} is close to 90% of the shear wave speed (c_s) produced the observed injection vein orientations. Here we show that by considering the observed injection vein lengths we can further constrain these scenarios, thereby limiting the source parameters to a narrow range of values for the rupture parameters L, R, D_c, and $\sigma^0_{yx} - \tau_r$. The idea is that the transient tensile stress associated with the propagating earthquake rupture should be just large enough to allow tensile cracks and/or injection veins with the observed lengths and orientations to grow during the rupture. Therefore, if one can constrain the near-tip stress fields accounting for the tensile cracks and/or injection veins while simultaneously satisfying all boundary conditions of the model, the source parameters of the model should reflect those of the earthquake rupture. We first show that this approach works for laboratory earthquake experiments, and then we scale the approach to the Gole Larghe fault zone.

EXPERIMENTS

Griffith et al. (2009) investigated the development of tensile crack arrays in the vicinity of a dynamically propagating earthquake rupture by producing ~M_w 4 sub-Rayleigh (slower than the Rayleigh wave speed, c_R) shear ruptures in Homalite-100 (density ρ = 1200 kg m^{-3}, dynamic elastic modulus E = 3.5 GPa, and Poisson's ratio ν = 0.26) plates along a pre-cut, bonded interface inclined at angle α to an applied uniaxial stress P (Fig. 1). These experimental shear ruptures produced damage zones consisting of arrays of tensile cracks that nucleated and grew dynamically in triangular zones behind the tip of the propagating shear rupture on one side of the fault interface (Figs. 1, 2A, and 2B). Near-tip stress fields were captured in photos of photo-elastic fringe patterns, which are contours of maximum shear stress (Fig. 3A). Using a semi-infinite mode II crack model with a velocity-weakening law, Ngo et al. (2012) showed that the orientation of these cracks is controlled by rupture velocity, v_{II}, and static prestress state.

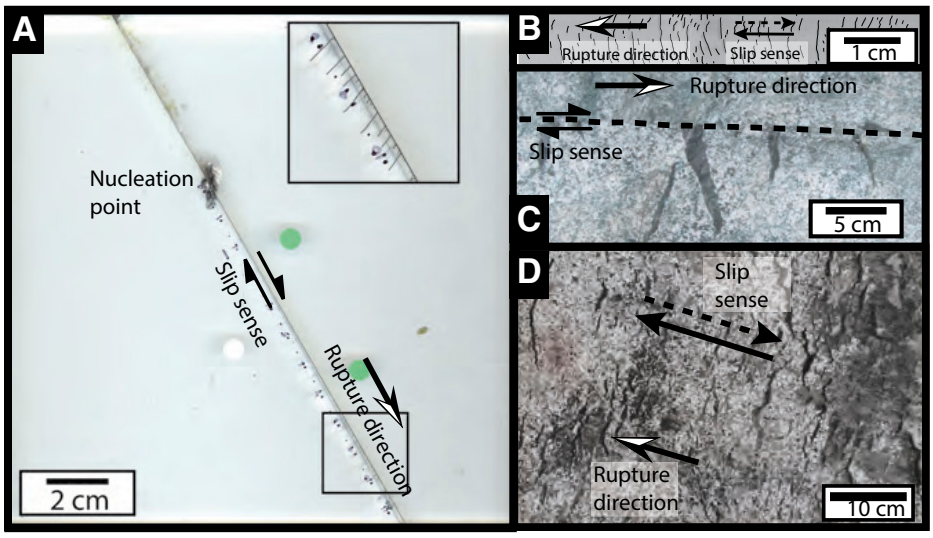

Figure 2. Comparison between microcracks from experiment 60I of Griffith et al. (2009) and injection veins in Gole Larghe fault zone (GLFZ, southern Italian Alps). A: Side view showing length of microcracks generated in Homalite-100 plates. B: Microcracks viewed on the sliding plane. C: Injection veins from GLFZ viewed on a cross-section plane parallel to slip direction. D: GLFZ fault surface view of injection veins. Slip direction given by paired arrows, and rupture direction given by single arrow.

In their experiments on Homalite-100 Griffith et al. (2009) measured shear rupture velocity v_{II}, σ^0_{yx}, and σ^f_{yx}, and showed that the recovered shear stress σ^f_{yx} is always less than σ^0_{yx}; therefore, the measured $\sigma^0_{yx} - \sigma^f_{yx}$ places a lower bound on the dynamic stress drop ($\sigma^0_{yx} - \tau_r$). In similar laboratory experiments, Lu et al. (2007) measured total slips <1 mm, so we take 1 mm to be an upper bound for S. There are several unknown parameters (R, L, and $\sigma^0_{yx} - \tau_r$), but once they are evaluated, D_c and G can be found from the model (Rice et al., 2005).

In this regard, several constraints on the near-tip stress fields are available from the experiments discussed here. First, the photo-elastic images provide the length l_c of the zone of actively developing microcracks of length l (Fig. 3A). Microcracks initiate a distance l_E behind the rupture tip and continue to grow along the trailing edge of the slip zone up to $x = -(l_c + l_E)$. To estimate l_c, we consider the distance behind the rupture tip where the local stress intensity factor K^d_I at the crack tips falls below the value necessary for crack propagation. For the experiments of Griffith et al. (2009), this happens when the crack-perpendicular tensile stress falls below ~5 MPa (Fig. DR1 in the GSA Data Repository[1]). In addition, photo-elastic fringe patterns can be reproduced based on the computed near-tip stress fields for each set of frictional parameters and compared to the high-speed photo-elastic images (Fig. 3C). Finally, the measured microcrack inclination angle should match the local trajectory of maximum compressive stress (Fig. 3D). The correct combination of $\sigma^0_{yx} - \tau_r$, L, and R should match all three experimental observations.

We explore all possible combinations of these parameters for total slip $\lesssim$1 mm for $\sigma^0_{yx} - \tau_r$ = 2.5 MPa, 3 MPa (Fig. 4A), and 3.5 MPa, respectively (Fig. DR2). Microcracks were observed to form at inclination angles of $\theta \approx 80°$ to the main rupture, and l_c was ~1.5 cm (Fig. 3A). Note that due to the high inclination angle, the relationship between l_c and maximum crack length l can be approximated by $l = l_c \tan\theta$, and the tensile crack velocity v_I within the triangular growth zone (Fig. 1) can likewise be related to shear rupture velocity v_{II} by $v_I = v_{II} \tan\theta$. We contour the predicted l_c based on the size of the tensile zone associated with the slip pulse model using combinations of R, L, and $\sigma^0_{yx} - \tau_r$, and identify cases for which 1 cm ≤ l_c ≤ 1.5 cm (Fig. 4A; Fig. DR2). Several parameter combinations in the range of 3 MPa ≤ $\sigma^0_{yx} - \tau_r$ ≤ 3.5 MPa, 6 cm ≤ L ≤ 10 cm, and 0.1L cm ≤ R ≤ 0.3L cm are able to match the observed l_c (Fig. 4A; Fig. DR2). Of the model parameter ranges that fit l_c (Figs. DR2 and DR4), the best theoretical fit to the experimental fringe patterns is provided by the model with $\sigma^0_{yx} - \tau_r$ = 3 MPa, L = 8.3 cm, and R = 0.83 cm, resulting in a slip weakening distance D_c ≈ 130 μm (Fig. 3C). This model also provides a good fit to observed tensile crack inclination angle (Fig. 3D).

GOLE LARGHE FAULT ZONE

A comparison between the experimental tensile cracks observed on a sliding plane of a post-mortem specimen and injection veins viewed on an exhumed fault surface in the Gole

[1]GSA Data Repository item 2015260, supplemental Figures DR1–DR7, is available online at www.geosociety.org/pubs/ft2015.htm, or on request from editing@geosociety.org or Documents Secretary, GSA, P.O. Box 9140, Boulder, CO 80301, USA.

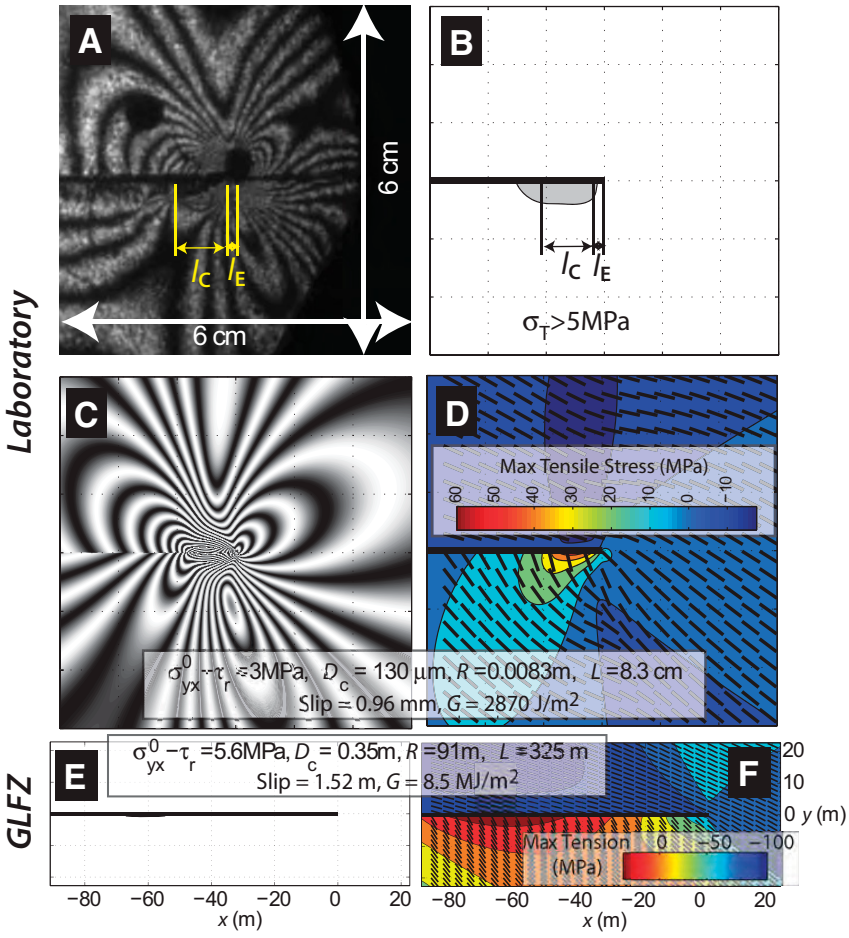

Figure 3. Constraints on length of zone of actively growing cracks (l_c) and resulting near-tip stress fields for fit to experiment 60I (A–D) and the Gole Larghe fault zone (GLFZ, southern Italian Alps) (E–F). A: Fringe patterns around rupture tip showing active crack formation. B: Extent of region with crack-perpendicular tensile stress σ_T > 5 MPa (gray). Scale is identical to that of A. C: Theoretical fringe patterns based on computed near-tip stress field. D: Near-tip maximum tensile stress field (contours) overlain by directions or maximum compressive stress. Plots in B–D are based on parameters listed at bottom of C and D in inset. For experiment 60I, inclination angle α = 60° and pressure P = 31.3 MPa. A static stress drop of 1.8 MPa was observed during the experiment. E: Extent of region with $\sigma_T \geq$ 10 MPa for GLFZ for parameters given in inset. F: Near-tip maximum tensile stress field (contours) overlain by directions of maximum compressive stress for same parameter combinations and spatial extent as in E. l_E is the length of the zone of elastic deformation preceding crack growth.

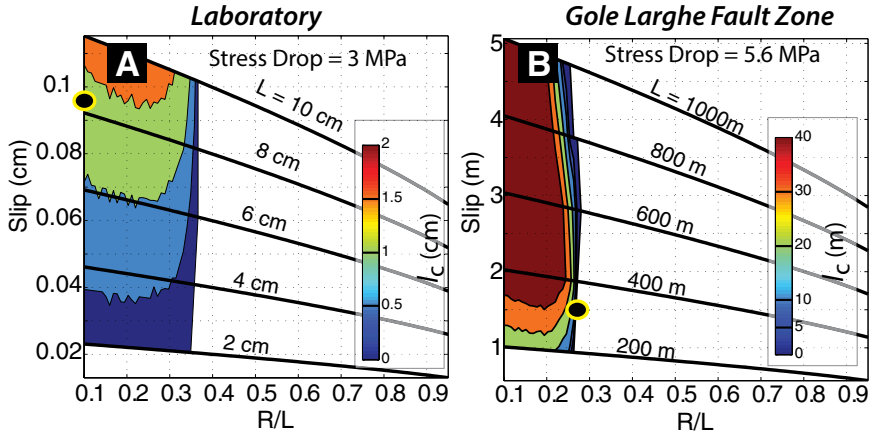

Figure 4. Relationship between slip and *R*/*L* for fixed values of pulse length *L* and slip weakening zone length *R* for experiment 60I of Griffith et al. (2009) (A) and Gole Larghe fault zone (southern Italian Alps) (B). Color contours show predicted values of length of zone of actively growing cracks (l_c) using method described in text. Yellow circles indicate parameter combinations shown in Figure 3.

Larghe fault zone reveals several striking similarities (Fig. 2; Fig. DR3). In both examples, the cracks initiate and grow into the host material preferentially on one side of the fault, with the crack plane perpendicular to the slip direction. Viewed on the fault plane, both experimental and natural cracks are typically arcuate, with the convex side in most cases pointing in the rupture direction. As viewed on the fault plane, the cracks are discontinuous and overlap, and larger cracks are interspersed with more closely spaced smaller cracks (Fig. 2D). This explains the apparently random length distributions as viewed on cross-sectional planes parallel to the slip direction (Fig. 2B; Di Toro et al., 2005b). Furthermore, across a large exposed fault surface (Fig. DR3), injection veins form in discontinuous patches rather than being spread over the entire fault surface, suggesting that the stress field is not conducive to tensile failure during the entire rupture.

In order to extend the approach described above from laboratory earthquakes to the Gole Larghe fault zone, we convert the problem from plane stress (as in laboratory experiments) to plane strain for natural faults; further, we assume the static pre-stress state to be biaxial, corresponding to a critically stressed Andersonian strike-slip fault with a static friction coefficient of 0.75. Following Di Toro et al. (2005a) in choice of material properties and assuming hydrostatic pore pressure, the static pre-stress state is $\sigma_{xx}^0 = -208$ MPa, $\sigma_{yy}^0 = -112$, and $\sigma_{yx}^0 = 83$ MPa. Using this pre-stress state, we design rupture scenarios that produce coseismic slips of ~1.5 m with stress drops between 5.6 MPa and 15 MPa (Fig. DR2). We assume the injection vein lengths to reflect the original crack length formed during the rupture event. In many cases, the observed injection vein length is likely to be greater than the original crack length because of crack extension associated with injection of pressurized melt after the earthquake rupture tip has passed (Griffith et al., 2012). Consequently, the observed injection vein lengths are an upper bound on the length of the cracks formed under the influence of the propagating shear rupture tip. We use injection vein length of 0.5 m ≤ l ≤ 1 m, corresponding to the longest veins observed by Di Toro et al. (2005a) and Griffith et al. (2012) of ~0.5 m, and allowing for the possibility that the observed vein length in the 2-D outcrop exposure is an underestimate of the true vein length. We use the lack of branching observed in the injection veins (Griffith et al., 2012) to assume that the tensile cracks grew at $v_1 \leq 0.2c_s$, an approximate branching velocity for mode I fractures, and the shear ruptures grew at ~0.9 c_s. This yields l_c responsible for vein growth during the rupture of ~2–5 m (i.e., l multiplied by 9/2). Note that our choice of mode I crack velocity exerts a very small influence on the results of the study, and given that we use

the maximum observed vein length l, the true l_c values were probably smaller than our results would indicate. In other words, our results can be viewed as an upper bound. As in the experiments, we constrain possible combinations of $\sigma^0_{yx} - \tau_r$, L, and R by examining the effect of each parameter on the predicted l_c in the slip-versus-R/L parameter space, and compared to the experiments, the range of possible results is quite narrow (Fig. 4B; Fig. DR2). For a stress drop of 5.6 MPa, only slip pulses with $L \approx 325$ m and $R/L \approx 0.28$ m result in $l_c < 10$ m with total coseismic slip of 1.5 m (Di Toro et al., 2005b). Stress fields associated with these parameters are plotted in Figures 3E and 3F and result in $D_c = 0.35$ m and $G = 8.5$ MJ/m^2. At larger stress drops (Fig. DR2) the results are similar except that predicted R/L is larger, and at stress drops greater than 15 MPa, the predicted coseismic slip magnitudes that are consistent with l_c exceed 1.5 m. Accounting for all parameter combinations that match the slip distance and l_c observed in the field, the parameters governing the rupture pulses can be constrained such that 5.6 MPa $\le \sigma^0_{yx} - \tau_r \le$ 15 MPa, 200 m $\le L \le$ 325 m, 90 m $\le R \le$ 180 m, 0.35 m $\le D_c \le$ 0.74 m, and 8.5 MJ/m$^2 \le G \le$ 24 MJ/m^2 (Figs. 3E and 3F; Fig. DR7).

CONCLUSIONS

In this study we assumed that cracks hosting injection veins were formed by transient tensile pulses during earthquake ruptures and later (during the same rupture) intruded by melt formed on the sliding surface. For constant rupture velocity, vein length l depends on l_c. Using this assumption, we solved a complete boundary-value problem for pulse-like rupture on faults of the Gole Larghe fault zone, resulting in pulse properties 5.6 MPa $\le \sigma^0_{yx} - \tau_r \le$ 15 MPa, 200 m $\le L \le$ 325 m, 90 m $\le R \le$ 180 m, 0.35 m $\le D_c \le$ 0.74 m, and 8.5 MJ/m$^2 \le G \le$ 24 MJ/m^2. These results are profound in several respects. First, the field-based estimate of dynamic stress drop of ≤15 MPa, a D_c on the order of tens of centimeters, and fracture energies of 8.5–24 MJ/m^2 for ancient earthquakes agree with typical seismological estimates for modern earthquakes (Abercrombie and Rice, 2005; Cocco et al., 2009). Furthermore, the small size of L and R implies that for a rupture propagating near c_R (~3000 m/s), dynamic weakening is achieved in ~0.1 s or less. Also, with $S \approx 1.5$ m over slip pulses of a couple of hundred meters traveling near c_R, the implied slip rates are on the order of 10 m/s, much higher than seismic slip rates of 1 m/s often quoted in the literature (Cowan, 1999) and requiring rapid accelerations at the initiation of slip.

What insights do these field observations provide with regard to laboratory rock friction experiments? Stick-slip experiments with small total slip have yielded D_c ranging from several micrometers to hundreds of micrometers, whereas fast rotary shear experiments at normal stresses <25 MPa typically yield D_c on the order of meters, although extrapolating these results to larger normal stresses yield slip weakening distances on the order of tens of centimeters (Di Toro et al., 2011). More recent rotary shear experiments involving rapid accelerations result in D_c of several centimeters (Chang et al., 2012). Seismological estimates of D_c for large earthquakes typically lie somewhere between laboratory estimates (~0.5–1 m) (Cocco et al., 2009), and the magnitude of D_c seems to scale with S (Abercrombie and Rice, 2005), although seismological estimates of D_c are indirect calculations using the radiated energy and assuming simplified models relating D_c to fracture energy, G (e.g., Abercrombie and Rice, 2005). The apparent scale dependence of D_c may be explained by the observation that for a given peak slip rate, D_c depends on peak acceleration (Ohnaka, 2003). Stick-slip events during slow frictional sliding experiments experience very large peak accelerations and consequently small D_c, whereas rotary shear experiments with slowly varying or constant velocities exhibit much larger D_c (Ohnaka, 2003). Whether the answer lies in realistic normal stresses or accelerations, our results underscore the need to study frictional behaviors in the laboratory at fast slip rates, rapid accelerations, and large normal stresses. Thus far, experiments in this parameter space have been limited to rock analogue materials and very small slip (Yuan and Prakash, 2008a, 2008b).

ACKNOWLEDGMENTS

This work was supported by National Science Foundation grant EAR-1321598. The manuscript benefited from discussions with G. Di Toro and S. Nielsen and reviews by A. Schubnel, Bob Holdsworth, Marco Scuderi, and anonymous reviewers.

REFERENCES CITED

Abercrombie, R.E., and Rice, J.R., 2005, Can observations of earthquake scaling constrain slip weakening?: Geophysical Journal International, v. 162, p. 406–424, doi:10.1111/j.1365-246X.2005.02579.x.

Chang, J.C., Lockner, D.A., and Reches, Z., 2012, Rapid acceleration leads to rapid weakening in earthquake-like laboratory experiments: Science, v. 338, p. 101–105, doi:10.1126/science.1221195.

Cocco, M., Tinti, E., Marone, C., and Piatanesi, A., 2009, Scaling of slip weakening distance with final slip during dynamic earthquake rupture: International Geophysics, v. 94, p. 163–186.

Cowan, D., 1999, Do faults preserve a record of seismic slip? A field geologist's opinion: Journal of Structural Geology, v. 21, p. 995–1001, doi:10.1016/S0191-8141(99)00046-2.

Di Toro, G., Nielsen, S., and Pennacchioni, G., 2005a, Earthquake rupture dynamics frozen in exhumed ancient faults: Nature, v. 436, p. 1009–1012, doi:10.1038/nature03910.

Di Toro, G., Pennacchioni, G., and Teza, G., 2005b, Can pseudotachylytes be used to infer earthquake source parameters? An example of limitations in the study of exhumed faults: Tectonophysics, v. 402, p. 3–20, doi:10.1016/j.tecto.2004.10.014.

Di Toro, G., Han, R., Hirose, T., De Paola, N., Nielsen, S., Mizoguchi, K., Ferri, F., Cocco, M., and Shimamoto, T., 2011, Fault lubrication during earthquakes: Nature, v. 471, p. 494–498, doi:10.1038/nature09838.

Griffith, W.A., Rosakis, A.J., Pollard, D.D., and Ko, C.-W., 2009, Dynamic rupture experiments elucidate tensile crack development during propagating earthquake ruptures: Geology, v. 37, p. 795–798, doi:10.1130/G30064A.1.

Griffith, W.A., Mitchell, T.M., Renner, J., and Di Toro, G., 2012, Coseismic damage and softening of fault rocks at seismogenic depths: Earth and Planetary Science Letters, v. 353–354, p. 219–230, doi:10.1016/j.epsl.2012.08.013.

Lu, X., Lapusta, N., and Rosakis, A.J., 2007, Pulse-like and crack-like ruptures in experiments mimicking crustal earthquakes: Proceedings of the National Academy of Sciences of the United States of America, v. 104, p. 18,931–18,936, doi:10.1073/pnas.0704268104.

Ngo, D., Huang, Y., Rosakis, A.J., Griffith, W.A., and Pollard, D.D., 2012, Off-fault tensile cracks: A link between geological fault observations, lab experiments, and dynamic rupture models: Journal of Geophysical Research, v. 117, B01307, doi:10.1029/2011JB008577.

Niemeijer, A., Di Toro, G., Griffith, W.A., Bistacchi, A., Smith, S.A.F., and Nielsen, S., 2012, Inferring earthquake physics and chemistry using an integrated field and laboratory approach: Journal of Structural Geology, v. 39, p. 2–36, doi:10.1016/j.jsg.2012.02.018.

Ohnaka, M., 2003, A constitutive scaling law and a unified comprehension for frictional slip failure, shear fracture of intact rock, and earthquake rupture: Journal of Geophysical Research, v. 108, 2080, doi:10.1029/2000JB000123.

Rice, J.R., Sammis, C.G., and Parsons, R., 2005, Off-fault secondary failure induced by a dynamic slip pulse: Bulletin of the Seismological Society of America, v. 95, p. 109–134, doi:10.1785/0120030166.

Rowe, C.D., and Griffith, W.A., 2015, Do faults preserve a record of seismic slip: A second opinion: Journal of Structural Geology, v. 78, p. 1–26, doi:10.1016/j.jsg.2015.06.006.

Xia, K., Rosakis, A.J., and Kanamori, H., 2004, Laboratory earthquakes: The sub-Rayleigh to supershear rupture transition: Science, v. 303, p. 1859–1861, doi:10.1126/science.1094022.

Yuan, F., and Prakash, V., 2008a, Use of a modified torsional Kolsky bar to study frictional slip resistance in rock analog materials at co-seismic slip rates: International Journal of Solids and Structures, v. 45, p. 4247–4263, doi:10.1016/j.ijsolstr.2008.03.012.

Yuan, F., and Prakash, V., 2008b, Slip weakening in rocks and analog materials at co-seismic slip rates: Journal of the Mechanics and Physics of Solids, v. 56, p. 542–560, doi:10.1016/j.jmps.2007.05.007.

Manuscript received 12 March 2015
Revised manuscript received 8 June 2015
Manuscript accepted 16 June 2015

Printed in USA